JOURNAL OF AIRCRAFT
Vol. 44, No. 2, March–April 2007

Analysis of the Effects of Interference and Sealant on Riveted Lap Joints

Amarendra Atre* and W. S. Johnson†
Georgia Institute of Technology, Atlanta, Georgia 30313

Much of the fatigue damage in aircraft structures can be linked to the stress concentration arising at the rivet/skin interface in fuselage lap joints. Fatigue damage can degrade the strength of the structure and reduce structural integrity. Elastomeric adhesives and sealants are applied to the lap joints before riveting to prevent entry of moisture, thus, preventing corrosion. The effect of the sealant on the residual stress state resulting from the rivet interference and subsequent load transfer has not been investigated. A three-dimensional finite element model of the riveting process is simulated to determine the effects of interference and sealant on the induced stresses. Both implicit and explicit finite element techniques are utilized to model the process. The finite element simulation is validated initially for both techniques with experiment. The analysis with sealant shows an increase in the residual hoop stress for the majority of the cases in comparison to the results without sealant.

Nomenclature

A, B, C, m, n	=	material parameters
$D_{\max}$	=	deformed rivet head final diameter
E	=	elastic modulus
H	=	deformed rivet head final height
ε_p	=	plastic strain
$\varepsilon_{\text{true}}$	=	true strain
ε_y	=	yield strain
μ	=	Poisson's ratio
σ_{true}	=	true stress
σ_y	=	yield stress

I. Introduction

AIRFRAME teardown inspections are an effective means to learn about aging issues in older airframes. Such inspections provide essential data and information for aircraft structures susceptible to widespread fatigue damage. The Federal Aviation Administration and Delta Airlines (DAL) have teamed in a three-year effort to conduct destructive evaluation and extended fatigue testing of a retired Boeing 727 passenger aircraft near its design service goal.[1] Nine lap-spliced panels representative of fuselage structure susceptible to fatigue damage were removed from the aircraft to measure the development of cracks that initiated from service operations. Preliminary nondestructive inspection revealed a large number of cracks in the fuselage lap joint at the rivet/skin interface.[1] The presence of these cracks was attributed to the residual stresses generated during rivet installation. Furthermore, the presence of cracks was not consistent throughout the panels.

Airframe lap joints are treated with elastomeric sealants and adhesives before riveting. Thin layers of sealant can aid in preventing corrosion[2] by inhibiting moisture ingestion into the joint. The teardown inspection conducted by DAL revealed significant variations in rivet interference through the lap joint combined with variations in sealant thickness and presence of embedded drill shavings in the sealant, all of which could have contributed to the concentrated stress state leading to fatigue damage.[3,4] Figure 1 shows two such rivet sections obtained from the lap joint. Evident from Fig. 1a is the difference in rivet interference, deformation of sealant, and the presence of drill shavings.

Motivated by teardown inspections and laboratory nondestructive examinations of the fuselage lap joints, this research is targeted at analyzing the localized stress conditions at the rivet/skin interface resulting from rivet installation and subsequent load transfer in the presence of sealant. Finite element analysis serves as a good method for characterizing the stress state resulting from this large-deformation forming process. This is a follow-on paper to previous work conducted by the authors on stress analysis of riveted unsealed joints with manufacturing process variations.[5] In this paper, the finite element simulations take into account variations in rivet interference, sealant coverage, and the presence of drill shavings. The results are compared to baseline model without a sealant to observe the differences in the stress state at the rivet/skin interface. The results are interpreted in relation to nucleation and propagation of fatigue damage in riveted lap joints. The local residual stress state from the analyses also serves as a link-up to a global three-rivet row lap-joint model that can be implemented to study the mechanics of load transfer and establish design-based criteria for the fatigue performance of the structure. Because the sealant acts a soft material confined between two stiffer materials, the distortion of the sealant that occurs during the process presents a significant problem even to commercial finite element codes. Hence, both implicit and explicit finite element techniques are utilized to approximate the sealant behavior. The implicit scheme presents an easier method in solving quasi-static problems but is limited in its ability to model excessive element distortion. The explicit scheme, on the other hand, presents a superior capability to model large deformations but introduces inertia effects in the solution that must be taken into account when analyzing results.

II. Background

Significant research has been conducted on riveted lap joints without sealant to characterize the residual stress state resulting from the riveting process. Experimental techniques have shown limited success in providing an accurate representation of the residual stresses at the rivet/skin interface.[6–14] Finite element methods have been utilized to observe effects of rivet squeeze force on the resulting stress state with some success.[6,15–19] The majority of the finite element models are two-dimensional axisymmetric and cannot characterize the unsymmetric rivet deformation resulting from manufacturing process variations.[5] For two-dimensional models, the residual stress state resulting from rivet installation must be imported to subsequent models or rivet-clamping force must be applied[20–23] to observe the

Received 20 June 2005; revision received 14 October 2005; accepted for publication 21 October 2005.

*Graduate Researcher, The George W. Woodruff School of Mechanical Engineering, 801 Ferst Drive North West.

†Professor, The George W. Woodruff School of Mechanical Engineering, 801 Ferst Drive North West; steve.johnson@mse.gatech.edu.

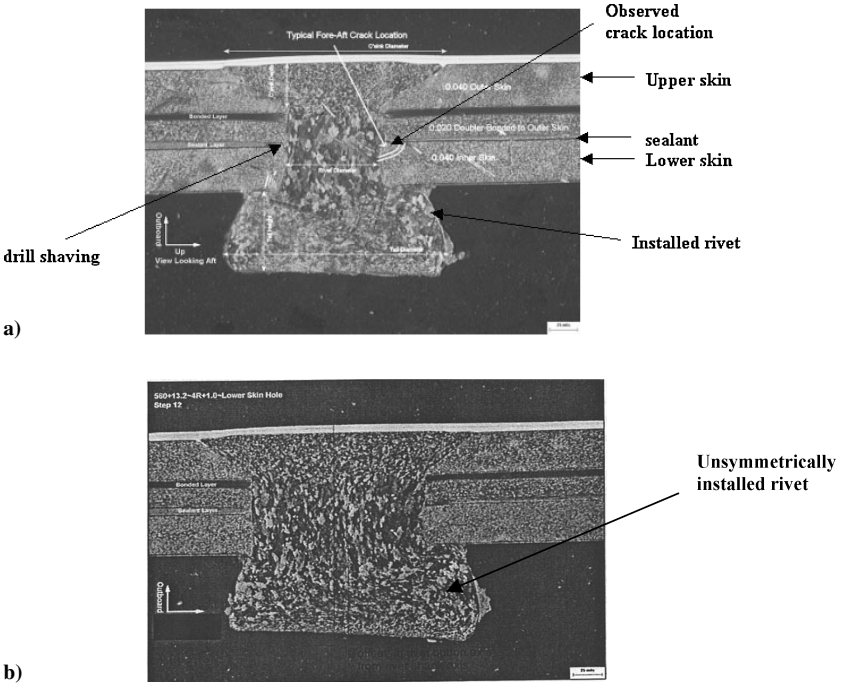

Fig. 1 Microscopy of riveted sections in lap joint.[3,4]

effects of load transfer.[24,25] Three-dimensional finite element models analyzed assume uniform interference and arbitrary estimates of clamping constraint provided by the installed rivet.[26]

For riveted lap joints with sealant, Imanaka analyzed the fatigue strength of adhesive-rivet lap joints experimentally.[27] He also investigated the stress distribution in the riveted joint for a high-modulus adhesive using the finite element method. Similar analysis was also conducted by Liu and Sawa[28] to evaluate the strength of single-lap adhesive joints with rivets, subjected to external bending moments. Dechwayukul et al.[29] presented a thin adhesive layer analysis finite element method to investigate the effects of thin sealant layers on the fatigue performance of riveted countersunk and noncountersunk lap joints. They compared their results to riveted lap joints without sealant and observed a reduction in the stress concentration factor at the rivet/skin interface. The analysis, however, does not take into account plasticity and the nonuniform interference produced by rivet installation.

III. Approach

In this study, the approach is as follows:

1) A two-dimensional axisymmetric quasi-static force-controlled finite element model of the riveting process is analyzed using ABAQUS/Implicit. The rivet deformation and force-displacement curves are validated with experimental measurements conducted by Li and Shi[30] on riveted lap-joint specimens to establish ABAQUS/Implicit capabilities.

2) A three-dimensional quarter-symmetry quasi-static finite element model of the riveting process is modeled in ABAQUS/Explicit. The resulting residual strains and the force-displacement curves are validated with experimental measurements conducted by Markiewicz et al.[31] on quasi-static riveted lap-joint specimens to establish ABAQUS/Explicit capabilities.

3) A three-dimensional baseline model of a quasi-static displacement controlled riveting process is constructed and analyzed in ABAQUS Implicit and Explicit based on lap-joint geometry data available from DAL. The results from both the solvers are compared to check the capability of the dynamic explicit solver to model the quasi-static riveting process.

4) The lap joints are sealed with elastomeric sealant or low-modulus adhesives. In ABAQUS/Implicit, the sealant is modeled as a solid low-modulus elastic material. In ABAQUS/Explicit, which provides superior contact and deformation capabilities, the sealant is modeled as a nonlinear hyperelastic material. Effects of differences in rivet interference and presence of drill shavings is also analyzed in both models.

5) Results are compared with analysis without sealant to observed effects on residual stress state.

IV. Results

A. Implicit Model Validation

The specimen configuration[30] analyzed in ABAQUS/Implicit is shown in Fig. 2. It consists of two 76.2×76.2 mm bare 2024-T3 AL alloy sheets each 2 mm thick and one 2117-T4 Al alloy countersunk-type rivet MS20426AD8-9. The rivet has a total length of 14.2 mm and a shank diameter of 6.35 mm. The mean inner sheet hole diameter is 6.4 mm. The rivet's mean protruding height above the inner sheet surface is 9.9 mm. The material properties for the sheet and the rivet are implemented from the parameters obtained by uniaxial tensile tests on 2024-T3 and 2117-T4 aluminum alloy, respectively.[30] Tables 1 and 2 show the material property parameters for both the Al alloy sheet and the rivet used in the finite element models. A tabular input of the data is provided in ABAQUS/Standard 6.4-1 using Eq. (1) based on experimental data. The material model assumes isotropic hardening with linear interpolation performed by ABAQUS between data points,[32]

$$\sigma_{\text{true}} = C\left(\varepsilon^{m}_{\text{true}}\right) \tag{1}$$

A detailed view of the meshed axisymmetric finite element model and the applied boundary conditions is shown in Fig. 3. The model, which has 8214 nodes and 7254 elements, is generated using ABAQUS/CAE 6.4-1 with CAX4R reduced integration four-node axisymmetric elements.[32] Three deformable bodies, two sheets and a rivet, and one rigid analytic tool are defined in the model. Geometric and surface interaction nonlinearities are included in the model. Surface interactions are defined as contact pairs using the master–slave algorithm available in ABAQUS/Standard with the finite sliding option. The surface contact is defined between the rivet and skin, rivet and the rigid tool, and between the upper and lower skin surfaces. The constraint applied by the tool that constrains the head of the rivet is modeled indirectly using boundary conditions. This improves convergence as well as saves computational time. The contact interaction is modeled with the coulomb friction

model. A coefficient of friction of 0.2 was specified for all surface interactions. Formulation of the elemental stiffnesses based on current configurations from deformed nodal positions is provided using the NLGEOM option, which means a geometric nonlinear analysis. Because the model undergoes large displacements, the calculated stresses are then the true stresses.

The skin edge surfaces on one end are constrained in the x direction with the y direction nodes constrained at the top and bottom to prevent rigid-body motion. The rivet displacement is fixed at the head while the squeeze force is applied at the rigid tool in contact with the rivet shank. The process is simulated in two steps: a loading step in which the rivet is deformed by the applied force and an unloading step in which the rivet is allowed to spring back.

The final deformed rivet driven head diameter and final deformed rivet head height predicted by the finite element analysis is compared with experimental measurements for the range of squeeze forces. These parameters are shown in Fig. 4 whereas Table 3 shows the comparison. Figure 5 shows the final rivet deformations after unload for a range of applied squeeze forces. Figure 6 shows a comparison of the force-displacement response from experiment to that predicted by the finite element method (FEM) for a squeeze force of 26.69 kN.

A maximum difference of 3.4% is observed for the final deformed rivet diameter whereas a maximum difference of 1.3% was observed for the final rivet height. The reasonable agreement of the rivet head

Table 1 Material property parameters used in finite element models

Elastic properties		Flow stress parameters		
E, GPa	ν		C, MPa	m
		Al 2024-T3[30]		
72.4	0.33	$\varepsilon_y \le \varepsilon_{\text{true}} \le 0.02$	765	0.14
72.4	0.33	$0.02 \le \varepsilon_{\text{true}} \le 0.1$	744	0.164
		Al 2117-T4,[30] *Al 2017-T4*		
71.7	0.33	$\varepsilon_y \le \varepsilon_{\text{true}} \le 0.02$	544	0.23
71.7	0.33	$0.02 \le \varepsilon_{\text{true}} \le 0.1$	551	0.15

Table 2 Material property parameters

Elastic properties		Flow stress parameters		
E, GPa	ν	A, MPa	B, MPa	n
		Al 2024-T351[33]		
74	0.33	350	600	0.502
		Al7050[33]		
74	0.33	312.5	290.5	0.25

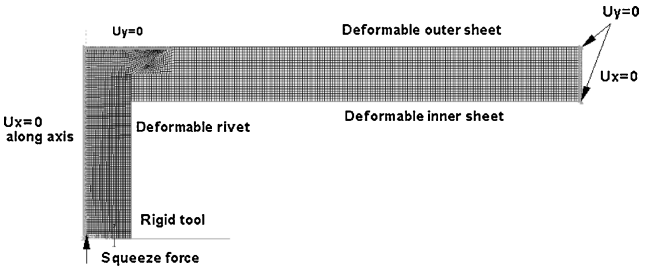

Fig. 3 Meshed view of axisymmetric model and applied boundary conditions.

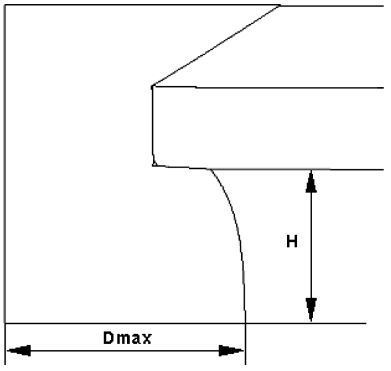

Fig. 4 Deformed rivet parameters.

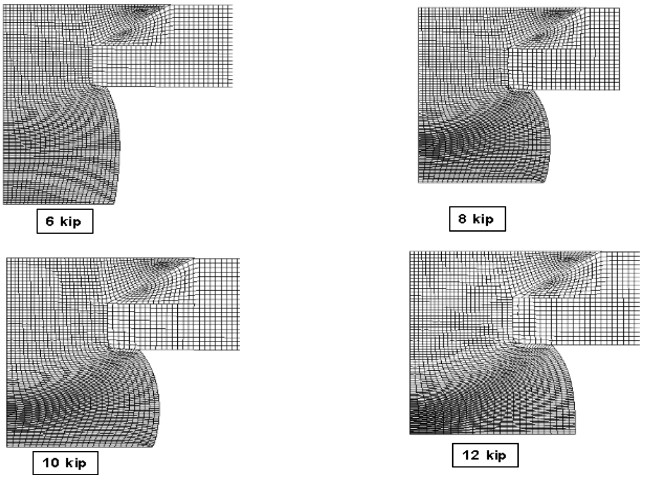

Fig. 5 Deformed configuration for range of applied squeeze forces.

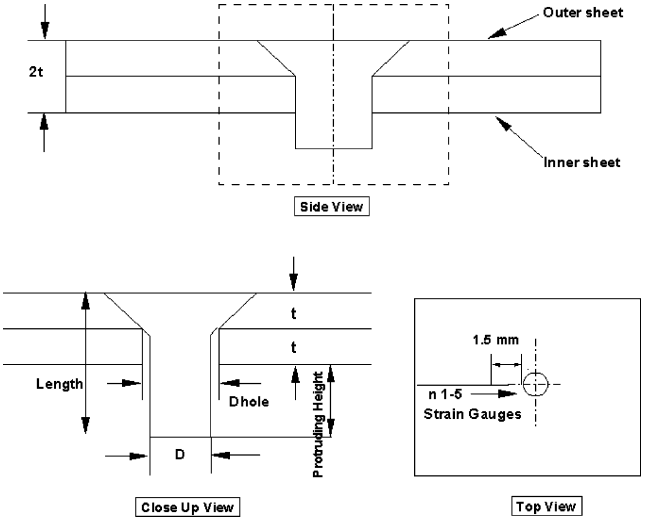

Fig. 2 Specimen configuration analyzed for ABAQUS/Implicit validation.[30]

Table 3 Comparison of rivet head deformation as predicted by the FEM to experiment

Squeeze force, kN	D_{max} FEM, mm.	D_{max} experiment,[29] mm.	% difference	H FEM, mm.	H experiment,[29] mm.	% difference
26	7.62	8.38	3.4	5.58	5.74	0.7
35	8.89	9.52	1.6	4.54	4.59	0.9
44	9.9	10.16	2	4	4.09	1.3
53	10.41	10.795	1.5	3.47	3.49	0.362

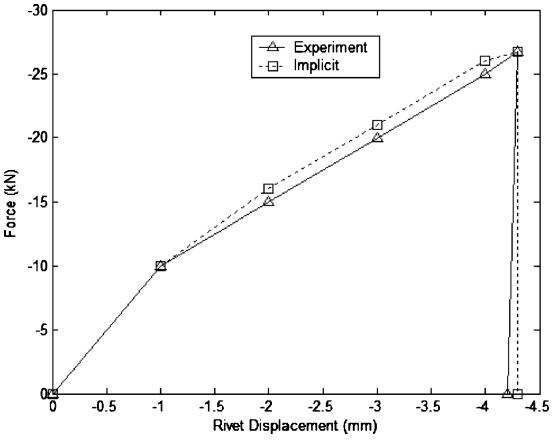

Fig. 6 Comparison of force-displacement curve for squeeze force of 26.69 kN for implicit solution.

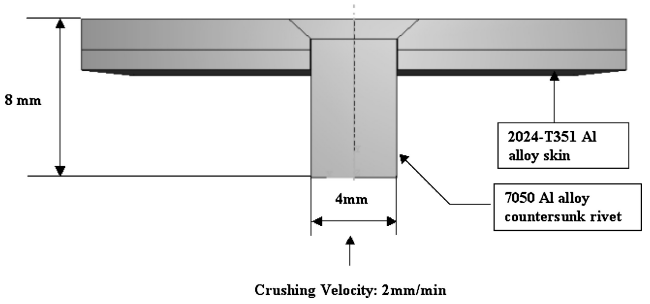

Fig. 7 Riveted joint parameters for model validation in ABAQUS/Explicit.

deformation as predicted by FE analysis and comparison of force-displacement curves with experiment demonstrates the capabilities of the solver to simulate the riveting process.

B. Explicit Model Validation

The specimen configuration[31] analyzed in ABAQUS/Explicit is shown in Fig. 7. It consists of two 15 × 15 mm bare 2024-T351 Al alloy sheets, each 1.6 mm thick, and one 7050 Al alloy countersunk-type rivet. The rivet has a total length of 8 mm. The material properties for the sheet and the rivet are implemented from the parameters obtained by experimental characterization[33] of 2024-T3 and 2117-T4 aluminum alloy, respectively (Table 1). A tabular input of the data is provided in ABAQUS/Standard 6.4-1 using Eq. (2) based on experimental data,

$$\sigma(\varepsilon_p) = A + B\varepsilon_p^n \tag{2}$$

The quarter-symmetry model, which has 31541 nodes and 22771 elements, is generated using ABAQUS/CAE 6.4-1 with C3D8R reduced integration four-node solid continuum elements.[32] Three deformable bodies, two sheets and a rivet, are defined in the model. Geometric and surface interaction nonlinearities are included in the model. The kinematic predictor–corrector algorithm is used in defining the surface interactions with a balanced master–slave approach. In this approach, the explicit solver applies acceleration corrections that are linear combinations of pure master–slave corrections. One

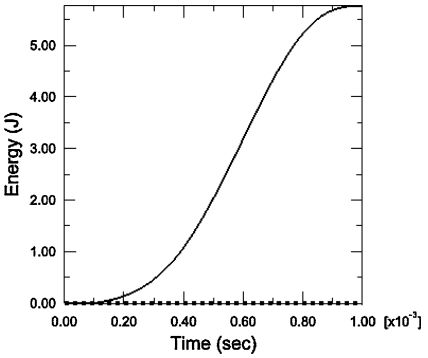

Fig. 8 Energy response in model: ——, internal energy and ∗∗∗∗, kinetic energy.

set of corrections is calculated considering one surface as the master surface, and the other corrections are calculated considering that same surface as the slave surface. Using this approach with hard kinematic contact minimizes surface penetrations that might occur during the process. The surface contact is defined between the rivet and skin and between the upper and lower skin surfaces. The constraint applied by the tool that constrains the head of the rivet is modeled indirectly using boundary conditions. The contact interaction is modeled with the coulomb friction model with a coefficient of friction of 0.2 assumed for all interactions. The skin edge surfaces on one end are constrained in the x direction with the y direction nodes constrained at the top and bottom to prevent rigid-body motion. A crushing velocity of 2 mm/min is applied to the rivet shank. The explicit solution is a true dynamic solution algorithm developed to model events in which inertia plays a significant role. Performing the analysis at a slow enough rate can ensure a quasi-static solution. If a simulation is quasi static, the work applied by the external forces is nearly equal to the internal energy of the system. Because inertia effects should be negligible in a quasi-static analysis as a general rule, the kinetic energy of the deforming material should not exceed a small fraction (typically 5–10%) of its internal energy throughout most of the process. Figure 8 shows a comparison of the energy response at the end of the riveting process. It can be seen that the kinetic energy is small enough in comparison to the internal energy for the solution to be considered quasi static.

The validity of the simulation is checked using three criteria. The von Mises stress of the deformed configuration and equivalent plastic strain at the end of analysis is compared to that predicted by Markiewicz et al.[31] The residual strains after riveting as predicted by finite element are compared to values recorded by strain gauges along the length of the skin.[31] The force-displacement response of the finite element solution is compared to the experimental response.[31] The von Mises stress predicted by the explicit solver (Fig. 9) is slightly lower than that predicted by Markiewicz et al.[31] The equivalent plastic strain, which provides a measure of the plasticity in the model, shows that the plastic strains in the rivet reach a range of 1.2 (Fig. 9). This is consistent to that reported by Markiewicz et al.[31] From comparisons of the residual strains (Fig. 10 and Table 4) it can be observed that the explicit and the finite element results are essentially in agreement. The explicit predicted force-displacement curve compared to experiment as in Fig. 11 also shows reasonable agreement. The finite element model predicts lesser elastic recovery than observed in experiment for both the implicit and explicit solutions.

Table 4 Comparison of residual strains

Gauge	Residual strain, Experiment	Residual strain, FE
1	0.01*e*–02	0.018*e*–02
2	0.04*e*–02	0.05*e*–02
3	−0.28*e*–02	−0.32*e*–02

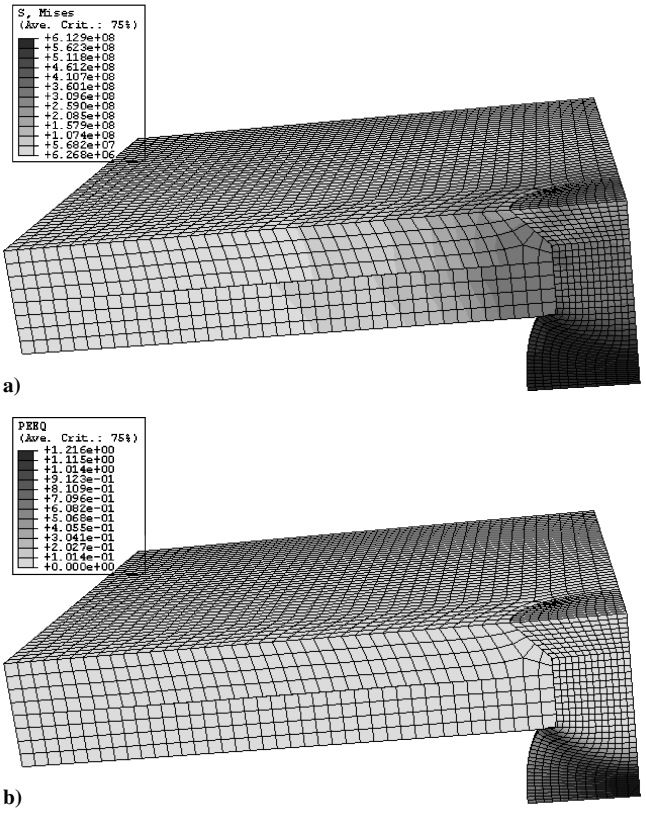

a)

b)

Fig. 9 Final deformed configuration: a) von Mises stress contour and b) equivalent plastic strains at end of the riveting.

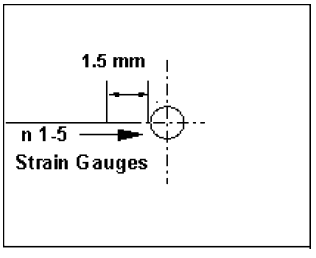

Fig. 10 Comparison of residual strains.

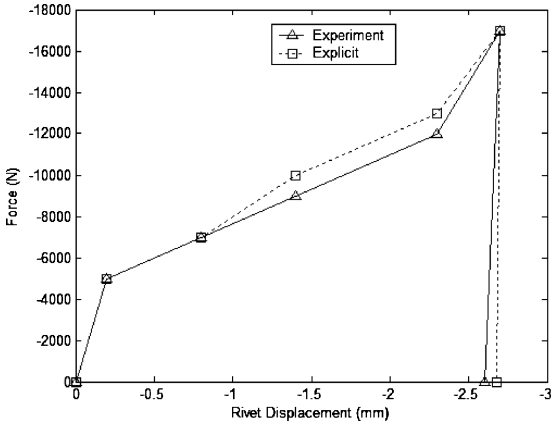

Fig. 11 Comparison of force-displacement diagram for explicit solution.

C. Baseline Model

Figure 12 shows the joint parameters modeled in this study from a personal communication with DAL, April 2004, in Atlanta, Georgia. The specimen configuration consists of two 2024-T3 25 mm × 25 mm Al alloy sheets. The upper skin is 1.5 mm thick and the lower skin is 1 mm thick. The 2017-T4 Al alloy countersunk-type rivet has a total length of 7.8 mm and a shank diameter of 3.9 mm. The lower skin hole diameter is 4 mm and the upper skin hole diameter is 6 mm at the top of the countersunk edge. The depth of the countersunk part measured from the top of the plate edge h_c is 0.09 mm. A coefficient of friction of 0.2 is assumed for lubricated contact and 1.1 for dry contact. The same friction coefficient is applied for both rivet/skin and skin/skin contact. The FE study is conducted as a quasi-static process (low speed). Any thermal and inertial effects are ignored.

A detailed view of the meshed, symmetric three-dimensional FE model and the applied boundary conditions is shown in Figs. 13 and 14. The model, which has 6457 nodes and 3947 elements, is generated using ABAQUS/CAE 6.4-1 with C38DR reduced integration eight-node linear solid brick elements.

The modeled riveting configuration is from the end of a three-row lap-joint. The skin edge surfaces on one end are constrained in the x direction with the y direction nodes constrained at the top and bottom to prevent rigid-body motion. The skin surfaces on the opposite end are unconstrained. The rivet displacement is fixed at the head, and a displacement of 3.3 mm is applied at the rivet driven head surface. Symmetric boundary conditions are imposed in the z direction for both the rivet and the skin surfaces. The process is simulated in three steps: a loading step in which the rivet is deformed by an applied displacement and an unloading step in which the rivet is allowed to spring back, followed by the bearing bypass loads for load transfer. The unloading step is important because at the end of the loading step the stress state is above yield at the rivet/skin interface, but after unloading most of these locations show a stress state below yield.

In ABAQUS/explicit the rivet-driven head displacement is applied using a smooth step loading amplitude function. Preliminary analysis showed that a time period of 0.001 s was appropriate to obtain a quasi-static solution and achieve computational efficiency. In all analyses it is ensured that the kinetic energy is negligible in comparison to the internal energy in the model. A small amount of material damping is also introduced in the explicit analysis to obtain a smoother kinetic energy response. Because explicit solutions typically require large run times compared to its implicit counterpart, it is not feasible to analyze both the loading and unloading steps in one analysis. Hence, for all of the explicit problems the rivet loading is analyzed in the solver, and the unloading step is completed in implicit using the IMPORT option provided by ABAQUS. In such analyses, the deformed configuration at the end of the explicit step is imported in implicit to conduct a static loading step. ABAQUS defines the imported stresses at the start of the analysis as the initial stresses in the material. Then, an additional set of artificial stresses is defined at each material point. These stresses are equal in magnitude to the imported stresses but are of opposite sign. The sum of the material point stresses and these artificial stresses, thus, creates zero internal forces at the beginning of the step. ABAQUS then ramps off of the internal artificial stresses linearly in time during the first step. Thus, at the end of the step the artificial stresses are removed completely, and the remaining stresses in the material are the residual stresses associated with static equilibrium. This is then followed by the application of tensile loads for load transfer where the load transfer ratio is defined as the ratio of load transferred to the upper skin (3.8 ksi) to the load applied to the lower skin (14.3 ksi).

Figure 15 shows the deformed plot and contours of residual hoop stress induced in the upper and lower skin after unloading in the original baseline implicit model. During the process, the rivet expands against the hole, and the contact pressure exceeds the yield point of the material, $\sigma_{11} < \sigma_y$. The material deforms so that $\sigma_{33} < 0$. This compressive hoop stress is analogous to cold working of holes with an expanding mandrel, carried out to prevent fatigue cracks that might initiate at the holes. The elastic deformation energy is

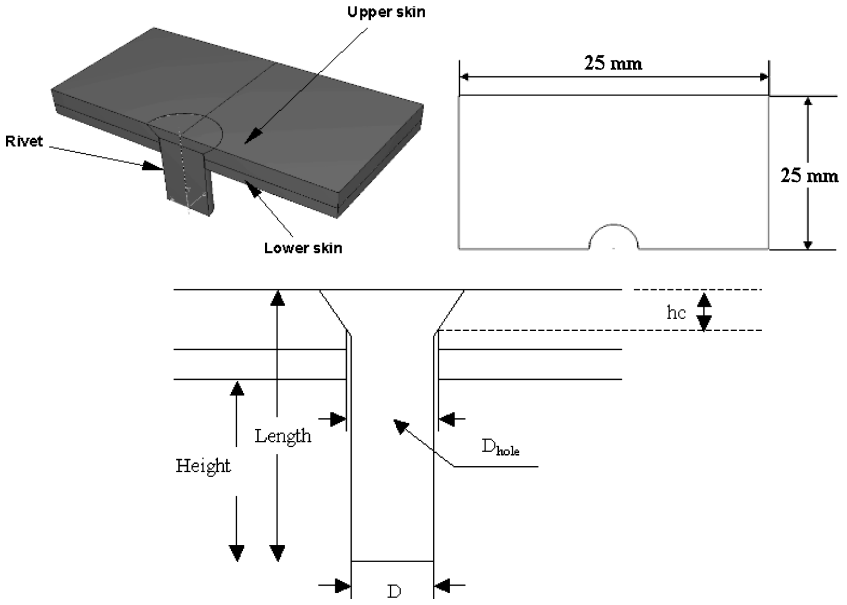

Fig. 12 Geometry parameters for baseline model.

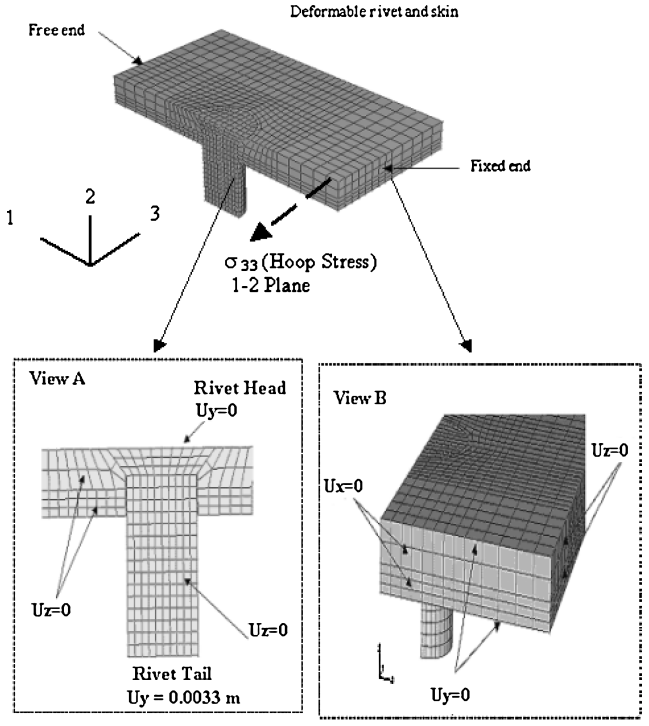

Fig. 13 Boundary conditions.

Table 5 Figure 15 hoop stresses

Hoop stress, MPa	Upper skin	Lower skin
Tensile	68	137
Compressive	−199	−351

not allowed full release after the process due to the large plastic deformation of the rivet. This leads to both compressive and tensile residual stresses in the skin. The compressive zone is balanced by the tensile zone away from the hole edge. This tensile hoop stress is critical for fretting fatigue cracks that may initiate at the faying surface. The hoop stresses shown in Fig. 15 and Table 5 are only on the face of the upper and lower skin.

The resulting interference is an indicator of the quality of the riveted joint. A high interference means a tighter connection between

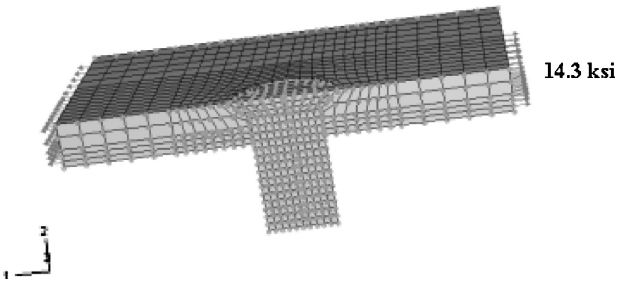

Fig. 14 Applied loads: rivet loading, unloading, and load transfer; load transfer Ratio = 38%, 3.8 ksi (upper) and 9.4 ksi (lower).

Table 6 Figure 17 hoop stresses

Hoop stress, MPa	Upper skin	Lower skin
Tensile	89	144
Compressive	−420	−599

the rivet and the skin. A larger compressive stress is observed for both the hoop and radial stresses in the lower skin than in the upper skin. As a result, the lower skin and the rivet are observed to have a tighter connection as compared to the upper skin. The residual stresses show a through-thickness variation as well as an unsymmetrical distribution. The resulting interference then also varies.

Figure 16 shows a comparison of the equivalent plastic strain in the implicit and explicit analysis. The results show a good agreement, indicating the ability of the dynamic solver to model the quasi-static problem. Figure 17 and Table 6 shows the residual stress state in the skin predicted by the explicit analysis. The residual stresses are qualitatively the same, but quantitatively the explicit solution shows approximately 20% larger values than that predicted by implicit. The difference in values must be taken in light of the dynamic nature of the solver based on stress wave propagation. Even though it is ensured that the analysis is quasi static, there will always be some inertia effects in the solution leading to the observed difference in residual stresses from the true quasi-static solution.

D. Analysis with Sealant

As stated earlier, the sealant analysis presents a large distortion problem. The element distortions that occur during the analysis combined with the nonlinear material model present a significant

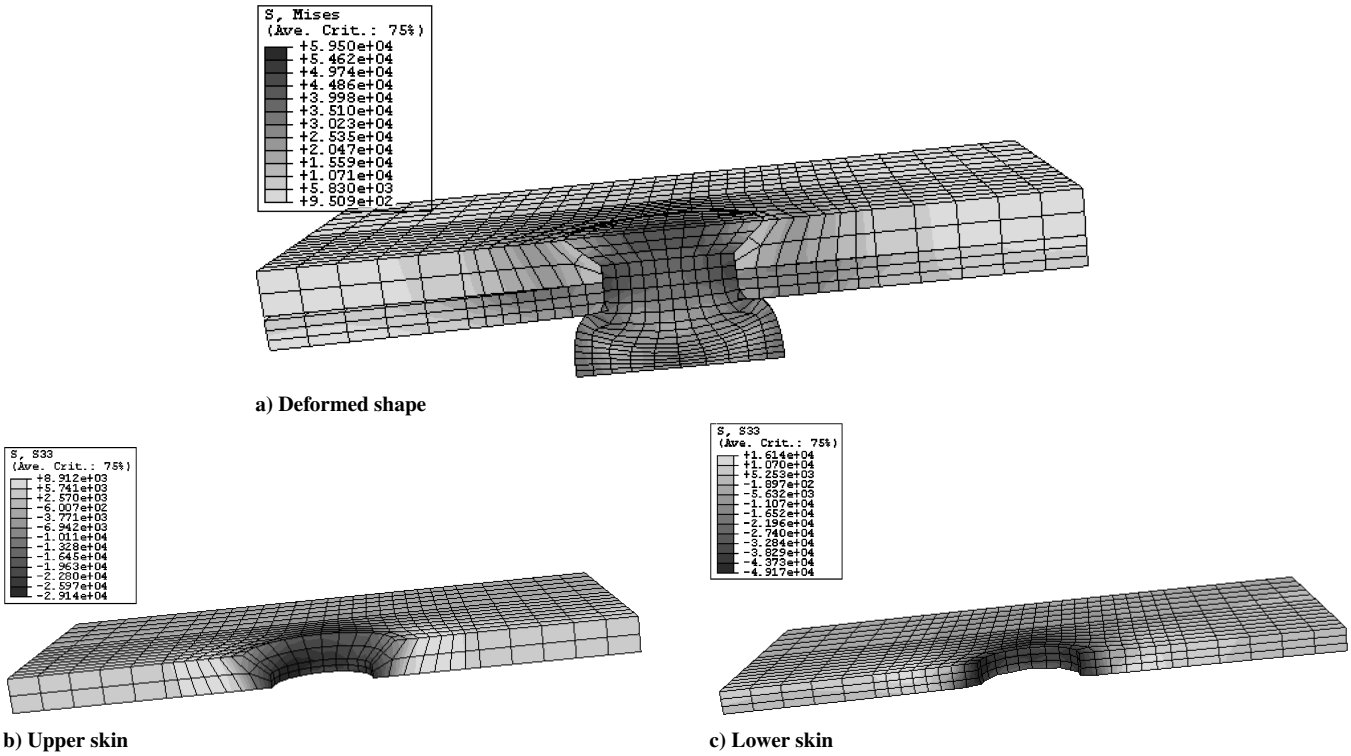

Fig. 15 Deformed shape and residual hoop stress contours in skin after unload in implicit analysis.

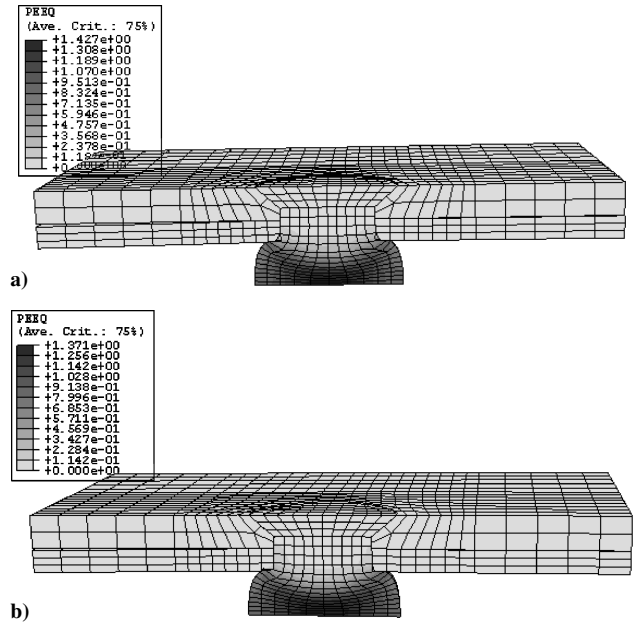

Fig. 16 Comparison of equivalent plastic strain from a) implicit and b) explicit.

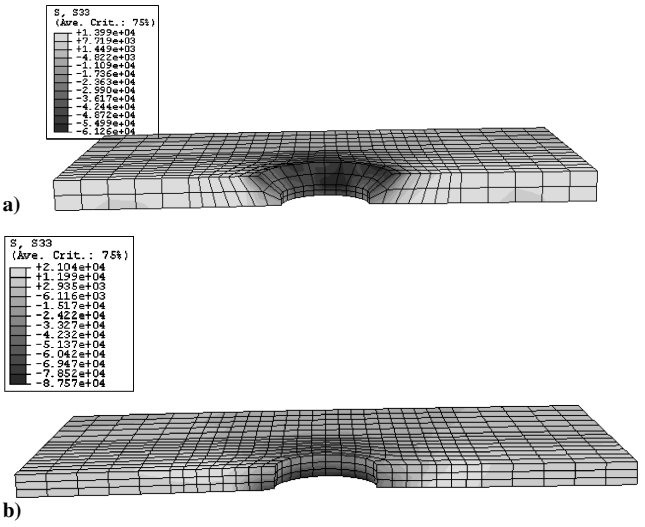

Fig. 17 Residual hoop stress contours in upper and lower skin as predicted by explicit analysis.

difficulty for the implicit solver, leading to explicit considerations. The sealant is modeled as a low-stiffness linear elastic adhesive material,[34] $E = 0.85$ GPa and $\nu = 0.31$, in implicit. In explicit, the sealant is modeled as a nonlinear hyperelastic material. The stress/strain data for the material and the evaluation of test data for different strain energy functions are shown in Fig. 18.

Elastomeric sealants are essentially incompressible materials. However, explicit requires a small amount of compressibility in the analysis. The amount of sealant compressibility is important when the material is confined between adjacent stiffer components. Larger compressibility ratios will introduce high-frequency noise in the solution, lead to excessively small time increments, and produce infeasible results. Trial analyses were conducted for Poisson's ratio ranging from 0.475 to 0.4999. A Poisson's ratio of 0.495 introduces the required compressibility in the solution without excessive run times. ABAQUS uses strain energy potential to relate stresses to strains for a hyperelastic material model from the test data provided. Several strain energy functions such as polynomial, Mooney–Rivlin, and Ogden are available. The test data were evaluated for the different strain energy functions. Evaluating the strain energy function is important because the material model might become unstable at certain strain magnitudes leading to convergence issues. A first-order polynomial strain energy potential was found to be stable for all strains and, hence, was implemented in the analysis. Figure 19 shows a view of the model with sealant. The sealant is modeled as a thin layer with a thickness of 0.127 mm. The sealant is constrained on one side whereas it is allowed to flow on the other side to capture the true effect. The sealant is modeled with C3D8R elements using enhanced hour-glassing options with distortion control to model the sealant deformation. Near the hole where significant

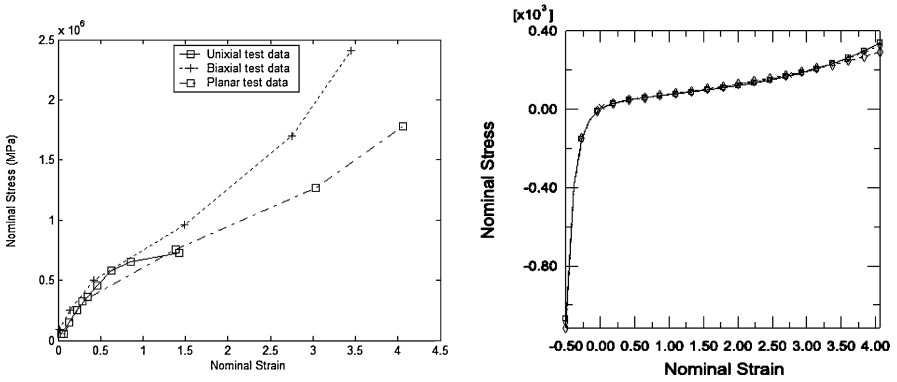

Fig. 18 Stress/strain data for hyperelastic material model: ——, OGDEN_N3 biaxial sealant_1; - - -, POLY_N1 biaxial sealant_1; - - -, POLY_N2 biaxial sealant_1; and ·····, test data biaxial sealant_1.

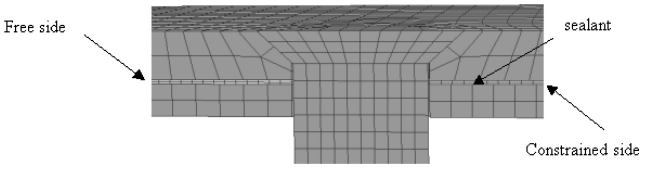

Fig. 19 FE model with sealant.

Table 7 Figure 21a hoop stresses

Hoop stress, MPa	Upper skin	Lower skin
Tensile	96	172
Compressive	−165	−344

Table 8 Figure 21b hoop stresses

Hoop stress, MPa	Upper skin	Lower skin
Tensile	213	179
Compressive	−393	−572

deformations are expected the sealant is modeled with a refined mesh through the thickness to minimize numerical errors. The model is implemented to observe the effects of interference and the presence of drill shavings on the residual stress state. For each case two simulations are conducted: one with the baseline interference, where the rivet is driven as per the specified standards, and one with low interference, where the rivet is underdriven as observed in the teardown inspection.

1. Baseline Interference and Sealant

Figure 20 shows the final deformed plot for both the implicit and explicit analyses. The explicit results show the true sealant deformation near the hole as seen from the microscopy of rivet installation. Figure 21 and Tables 7 and 8 show the residual hoop stress in the upper and lower skin for both of the analyses. For both the implicit and explicit cases, a quantitative increase in the tensile hoop stress for the upper skin (28 and 58%) and for the lower skin (19 and 23%) is observed. Qualitatively, the lower skin shows similar results whereas the upper skin shows a concentrated tensile stress near the countersunk edge.

2. Baseline Interference and Sealant Coverage Variation

The sealant coverage was reduced in an area next to the hole to observe the effect on the residual stress state. Figure 22 shows a deformed plot from the explicit analysis. For the baseline interference, no contact between the upper and lower skin is observed where the sealant coverage is reduced due to sealant flow taking place during riveting. The upper skin shows a shift in the tensile hoop stress near the countersunk edge. An increase in the tensile hoop stress is also

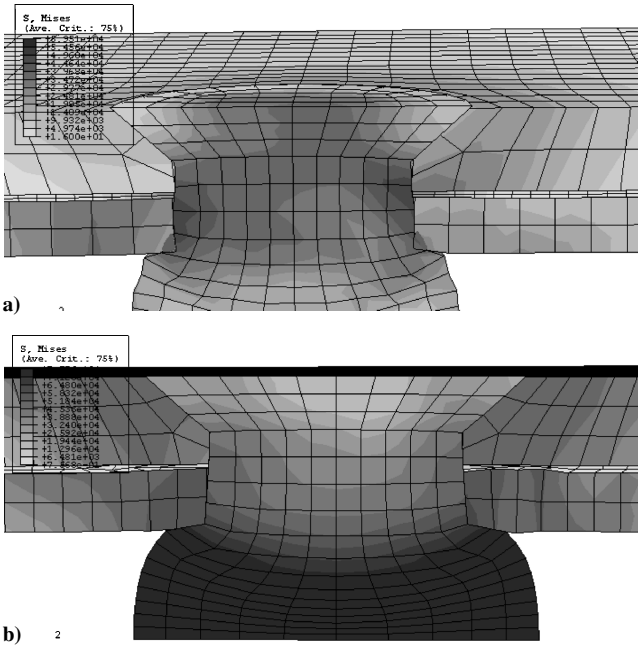

Fig. 20 Final deformed shape with sealant: a) implicit and b) Explicit.

observed for both the upper (76%) and lower skin (13%). For the implicit analysis, a converged solution could not be obtained.

3. Baseline Interference, Sealant, and Drill Shavings

Microscopy of the riveted lap joints revealed skin drill shavings embedded in the sealant. An analysis was conducted to observe the effects of baseline interference with embedded drill shavings present in the sealant. Figure 23 shows the FE model along with a representative rivet section. The drill shaving prevents the sealant flow near the hole and strongly affects the rivet deformation. For both the implicit and explicit cases, a quantitative increase in the tensile hoop stress for the upper skin (9 and 116%) and for the lower skin (5 and 47%) is observed.

4. Low Interference and Sealant

Figure 24 shows the final deformed plot for both the implicit and explicit analyses. In this case, the rivet is underdriven to obtain the effect of reduced interference. Both analyses show a dominant tensile hoop stress near the hole edge for the upper and lower skin. The explicit analysis shows a stronger tensile zone at the faying surface unconstrained side. In both analyses, a quantitative increase is observed for the tensile hoop stress in the upper skin (implicit 37.5% and explicit 81%) and lower skin (implicit 57% and explicit 29%) in comparison with the analysis for low interference without sealant (not shown).

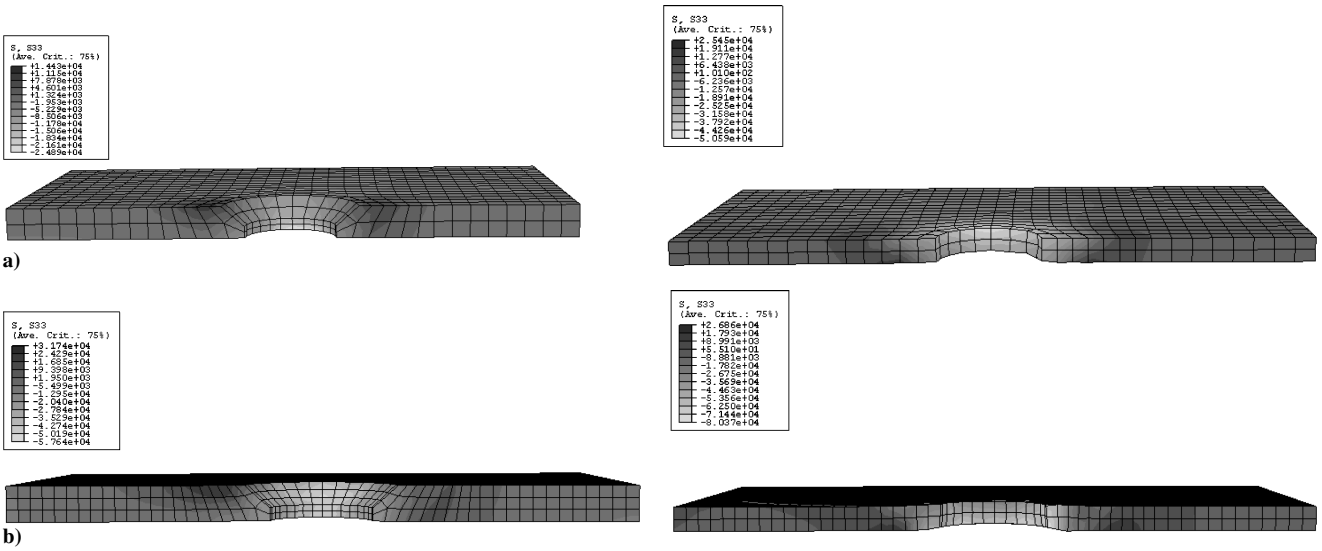

Fig. 21 Residual hoop stress contour in a) implicit and b) explicit for upper and lower skin.

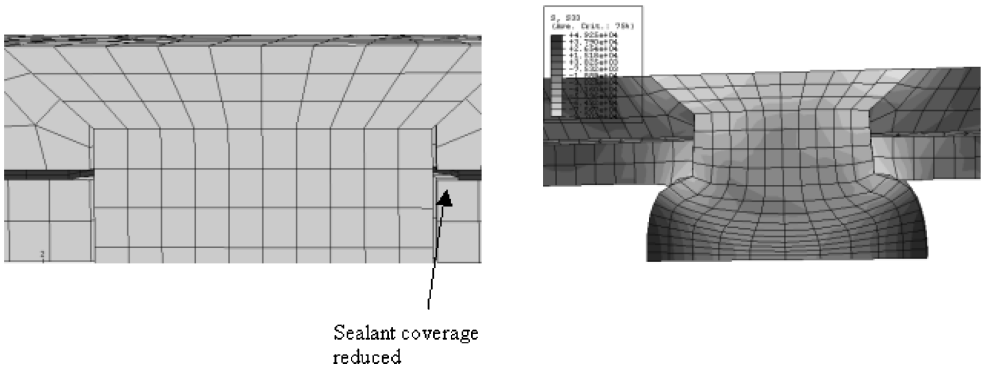

Fig. 22 Undeformed and deformed (explicit) plot showing reduction of sealant coverage.

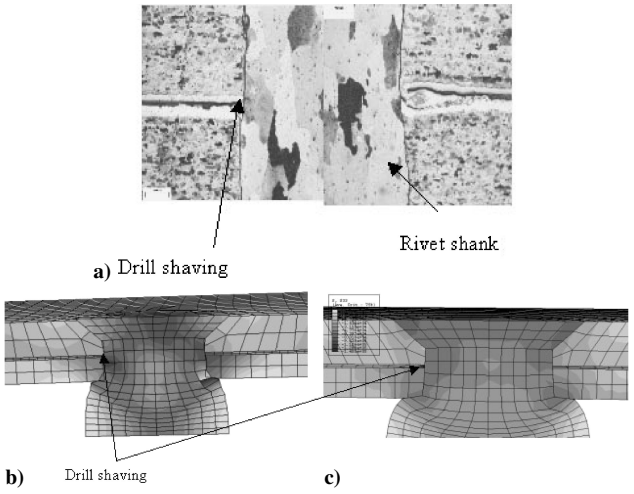

Fig. 23 Deformed plot: a) rivet section showing drill shaving and deformed plot of representative finite element model, b) implicit, and c) explicit.

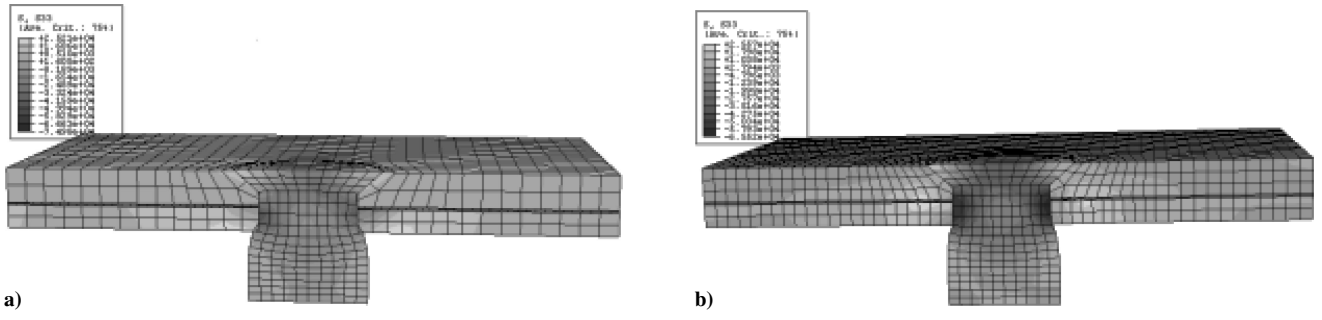

Fig. 24 Final deformed shape with sealant and low interference: a) implicit and b) explicit.

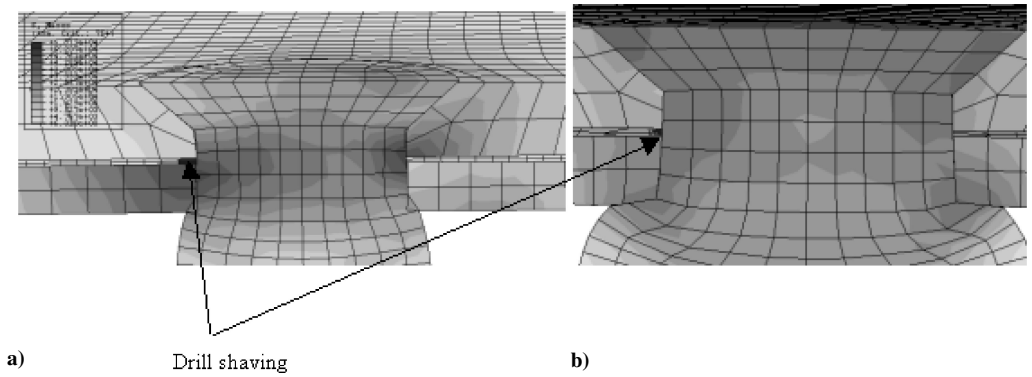

Fig. 25 Deformed plot of FE model for low interference and drill shavings: a) implicit and b) explicit.

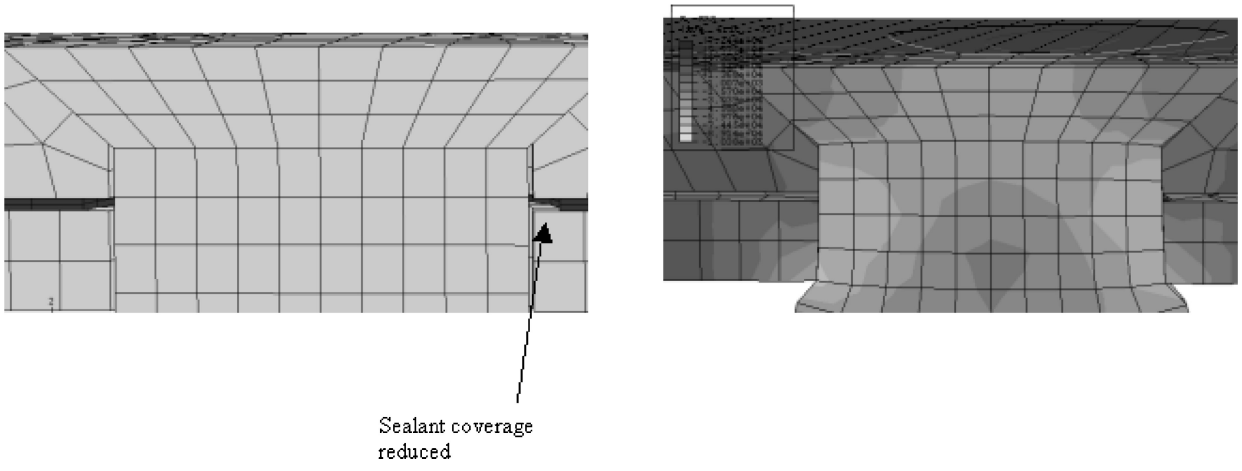

Fig. 26 Undeformed and deformed (explicit) plots showing reduction of sealant coverage for low interference.

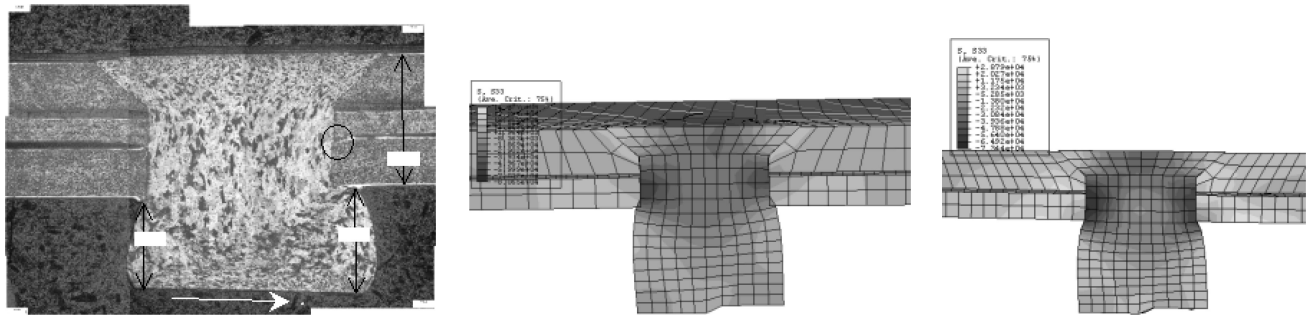

Fig. 27 Deformed configuration: a) rivet section showing rivet tilt and deformed plot of representative FE model, b) implicit, and c) explicit.

5. Low Interference, Sealant, and Drill Shavings

An analysis is conducted to observe the effects of low interference with embedded drill shavings present in the sealant. Figure 25 shows the FE model along with a representative rivet section. The tensile residual hoop stress remained concentrated near the holes at the rivet/skin interface with a quantitative increase of the residual tension in the upper skin (implicit 62% and explicit 109%) and in the lower skin (implicit 45% and explicit 47%).

6. Low Interference and Sealant Coverage Variation

In this case, the effect of low interference is analyzed with reducing the sealant coverage near the holes to observe the effect on the residual stress state. Figure 26 shows the deformed and undeformed plots in this case. Even for low interferences, the skin does not come into contact where the sealant coverage is reduced because of sealant flow in that area during the riveting process. Along with a quantitative increase in the tensile hoop stress for both the upper (109%) and lower (47%) skins, the tensile zone is also observed to shift inside the hole. For the analysis in implicit, even for the linear elastic adhesive model, a converged solution could not be obtained.

7. Rivet Tilt and Sealant

To simulate the rivet tilt (variation in rivet head deformation on opposite side of hole) observed from rivet microscopy, the applied rivet head displacement is varied in magnitude across the straight shank rivet head (point of application). Figure 27 shows an example of the rivet section and representative FE model. This method gives a first approximation of analyzing the residual stress state with an interference variation on both sides of the rivet hole. The residual hoop tension is observed to increase largely on one side of the hole for both the upper and lower skins.

V. Conclusions

One cause of fatigue damage in aircraft structures is stress concentration arising at rivet/skin interface in fuselage lap joints. A teardown inspection conducted by DAL on a retired B727 revealed

a large number of cracks in the fuselage lap joint at the rivet/skin interface. The teardown also showed variations in the installed rivets through the lap joint. The presence of these cracks was attributed to the stresses arising from the rivet installation combined with in service bearing and bypass loads. In this paper, three FE models of the lap joint have been analyzed to investigate the effect of rivet installation and subsequent loading on the localized stress state at the rivet/skin interface. The following are the conclusions from the study:

1) A two-dimensional axisymmetric FE model of a force-controlled riveting process has been simulated using ABAQUS/implicit. The resulting rivet head deformation and force-displacement curves have been compared with those recorded by experiment. A maximum difference of 3.4% has been observed for the rivet head deformation between the FE model and experimental measurements.

2) A three-dimensional one-quarter symmetry one-rivet quasi-static FE model of the riveting process has been modeled in ABAQUS/explicit. The resulting residual strains and force-displacement data have been validated with experiments. Furthermore, the von Mises stress and equivalent plastic strain predicted by the code have been compared to the model analyzed by Markiewicz et al.[31] A maximum difference of 20% has been observed for the residual strains between the FE model and experimental measurements. The maximum equivalent plastic strain in the rivet (1.2) is consistent with that reported by Markiewicz et al.[31] The kinetic energy response always remains within 10% of the internal energy response ensuring minimal inertia effects.

3) A three-dimensional baseline model of a two-rivet quasi-static displacement controlled riveting process that also takes into account the bearing bypass loads resulting from the load transfer between the rivet and skin has been constructed and analyzed in ABAQUS implicit and explicit based on lap-joint geometry data available from DAL. The three-dimensional analysis captures the unsymmetric deformation produced by rivet buckling and allows for easier modeling of load transfer effects wherein the modeled bearing bypass ratio was 38%. The results from both of the solvers have been compared to check the capability of the dynamic explicit solver to model the quasi-static riveting process. The maximum equivalent plastic strain in the rivet for both analyses has been observed to be the same (1.4). The residual stresses predicted by explicit are around 20% higher than those predicted by implicit. This difference in stresses can be attributed to the inertia effects produced by the dynamic solver. Qualitatively, the results agree in both cases.

4) The three-dimensional baseline model has been extended to include the effects of rivet interference with a sealant on the residual hoop stress. In implicit, the sealant has been modeled as low-modulus elastic adhesive, whereas in explicit a hyperelastic material model has been used. Results have been compared to the analysis without sealant. Importance has been placed in any qualitative variation in the residual hoop tension, particularly in the explicit analysis due to the inherent limitations of the solver in predicting stresses in the analysis.

5) The analyses with sealant show an increase in residual hoop tension for both the upper (20–80%) and lower (20–60%) skins.

a) For the cases where the rivet is driven as specified (baseline), the upper skin shows a shift in the tensile zone near the countersunk edge that might be a probable location for fatigue cracking. For the lower skin the tensile zone remains concentrated at the faying surface (away from the hole). For low-interference or underdriven rivets with the sealant, an increase in tensile hoop stress is observed with the tensile zone concentrated near the rivet/skin interface for both the upper and lower skin.

b) Rivet tilt also shows a similar tensile zone concentrated largely on one side of the hole due to the unsymmetric rivet deformation. For this type of installed rivets, the stress distribution seems to suggest that both the upper and lower skin would be susceptible to fatigue damage at the rivet/skin interface. Also for such cases the presence of sealant might not show any beneficial effects.

c) The effect of reduced sealant coverage between the upper and lower skin does not show any skin/skin contact due to sealant flow. For the baseline model the tensile stress zone is observed to shift near the countersunk edge, whereas for the low-interference case the tensile stress zone is observed inside the hole.

d) The presence of drill shavings in the sealant causes a large increase in the tensile hoop stress for both the upper (40–60%) and lower (50–110%) skins. The tensile hoop stress is also observed to remain concentrated at the rivet/skin interface for low interferences. Rivets installed with low interference (underdriven) and with drill shavings might be a major cause of fatigue crack initiation at the rivet/skin interface.

6) The presence of sealant shows an increase in the residual tensile stress state as compared to the analysis without sealant. For rivets that are installed per specifications (baseline), the effect of sealant on any fatigue damage might not be significant. For cases where rivets are underdriven or tilted the effects of sealant combined with any drill shavings might increase the propensity for fatigue crack nucleation at the rivet/skin interface.

Acknowledgments

The authors would like to thank John Bakuckas and Felix Abali at the Federal Aviation Administration for the financial support provided for this research and Delta Airlines for all of the technical data required for the analysis.

References

[1]Bakuckas, J. G., and Carter, A., "Destructive Evaluation and Extended Fatigue Testing of Retired Aircraft Fuselage Structure: Project Update," *Proceedings of the 7th Joint DoD/FAA/NASA Conference on Aging Aircraft*, Federal Aviation Administration, Washington, DC, 2003, pp. 1–12.

[2]Lucas, F. M., Silva, Goncalves, J. P. M., Oliveira, F. M. F., and de Castro, P. M. S. T., "Multiple Site Damage in Riveted Lap-Joints: Experimental Simulation and Finite Element Prediction, *International Journal of Fatigue*, Vol. 22, 2000, pp. 319–338.

[3]Radhakrishnan, R., "Damage Characterization," *Joint FAA/Delta 8th Quarterly Meeting on Destructive Evaluation and Extended Fatigue Testing of a Retired Passenger Aircraft*, Federal Aviation Administration, Washington, DC, 2004.

[4]Radhakrishnan, R., "Damage Characterization," *Joint FAA/Delta 10th Quarterly Meeting on Destructive Evaluation and Extended Fatigue Testing of a Retired Passenger Aircraft*, Federal Aviation Administration, Washington, DC, 2005.

[5]Atre, A., and Johnson, W. S.,"3-D FEA Simulations to Assess Residual Stresses in Riveting Processes," *Journal of ASTM International*, Vol. 3, No. 3, 2005, Paper ID: JAI13077.

[6]Muller, R. P.,"An Experimental and Analytical Investigation on the Fatigue Behavior of Fuselage Riveted Lap-joints," Ph.D. Dissertation, Dept. of Mechanical Engineering, Delft Univ. of Technology, Delft, The Netherlands, 1995.

[7]Markiewicz, E., Langrand, B., Deleotombe, E., Drazetic, P., and Patronelli, L.,"Analysis of the Riveting Forming Mechanisms," *International Journal of Materials and Production Technology*, Vol. 13, Nos. 3–6, 1998, pp. 123–145.

[8]Fitzgerald, T. J., and Cohen, J. B., "Residual Stresses in and Around Rivets in Clad Aluminum Alloy Plates," *Materials Science and Engineering*, Vol. A188, 1994, pp. 51–58.

[9]Nepershin, R. I., and Knigin, V. V., "Interferences and Residual Stresses in Riveted Joints," *Journal of Machinery, Manufacture and Reliability*, Vol. 5, No. 5, 1992, pp. 47–51.

[10]Yarkovets, A. I., Sirotkin, O. S., Firsov, V. V., and Kisilev, N. M., "Processes for Ensuring Long Life of Riveted and Bolted Joints in Aircraft Structures," *Mashinostroyeniye*, Moscow, 1987.

[11]Demina, N. I., and Volkov, A. K., "The Influence of the Interference of a Rivet on the Mechanical Properties of D16 Alloy Sheet in Biaxial Tension," *Cambridge Science Abstracts Aluminum Industry Abstracts*, Accession 01901145-0483, Vol. 21, No. 3, 1989, pp. 407–409.

[12]Ryzhova, T. B.,"Estimation of the Reliability of Ultrasonic Quality Control of Riveted Joints with Clearance," *Russian Journal of Nondestructive Testing*, Vol. 30, March 1998, pp. 418–421.

[13]Ryzhova, T. B.,"Ultrasonic Assessment of the Radial Clearance of Riveted Joints in Aircraft Structures," International Council of the Aeronautical Sciences, Paper ICAS-98-R, June 1998, pp. 1–7.

[14]Slater, W. J., "Static Strength of Riveted Joints in Fiber Metal Laminates," Ph.D. Dissertation, Dept. of Mechanical Engineering, Delft Univ. of Technology, Delft, The Netherlands, 1994.

[15]Szolwinski, M. P., and Farris, T. N.,"Linking Riveting Process Parameters to the Fatigue Performance of Riveted Aircraft Structures," AIAA Paper 99-1339, 1999, pp. 1208–1218.

[16]Deng, X., and Hutchinson, J. W.,"The Clamping Stress in a Cold Driven Rivet," *International Journal of Mechanical Sciences*, Vol. 40, Dec. 1998, pp. 683–694.

[17]Ryan, L., and Monaghan, J.,"Failure Mechanism of Riveted Joint in Fibre Metal Laminates," *Journal of Materials Processing Technology*, Vol. 103, Dec. 2000, pp. 36–43.

[18]Fung, C.-P., and Smart, J.,"An Experimental and Numerical analysis of Riveted Single Lap-joints," *Proceedings of the Institute of Mechanical Engineers-G-Journal of Aerospace Engineering*, Vol. 208, No. 2, 1994, pp. 79–90.

[19]Fung, C.-P., and Smart, J.,"Riveted Single-Lap-Joints. Part 1: A Numerical Parametric Study," *Proceedings of the Institute of Mechanical Engineers-G-Journal of Aerospace Engineering*, Vol. 211, No. 1, 1997, pp. 13–27.

[20]Harish, G., and Farris, T. N., "An Integrated Approach for Prediction of Fretting Crack Nucleation in Riveted Joints," AIAA Paper 99-1340, April 1999.

[21]Harish, G., and Farris, T. N., "Modeling of Skin/Rivet Contact: Application to Fretting Fatigue," *AIAA/ASME/ASCE 38th Structural Dynamics, and Materials Conference*, Vol. 4, AIAA, Reston, VA, 1999, pp. 2761–2771.

[22]Harish, G., and Farris, T. N., "Shell Modeling of Fretting in Riveted Lapjoints," *AIAA Journal*, Vol. 36, No. 6, 1998, pp. 1087–1093.

[23]Harish, G., and Farris, T. N., "Effect of Fretting Contact Stresses on Crack Nucleation in Riveted Lap-Joints," AIAA Paper 99-1340, 1998.

[24]Bellinger, N. C., Krishnakumar, S., and Komorowski, J. P.,"Modeling of Pillowing due to Corrosion in Fuselage Lap-Joints," *Canadian Aeronautics and Space Journal*, Vol. 40, No. 3, 1998, pp. 125–130.

[25]Shi, G., Bellinger, N., and Xiong, Y., "Three-Dimensional Nonlinear Finite Element Modeling and Analysis of Riveted Lap-Joints with Corrosion Pillowing," *Advances in Computational Engineering and Science*, Vol. 2, Feb. 2000, pp. 1542–1547.

[26]Iyer, K. A.,"Three-Dimensional Finite Element Analyses of the Local Mechanical Behavior of Riveted Lap-joints," Ph.D. Dissertation, Materials Science and Engineering, Vanderbilt Univ., Nashville, TN, May 1997.

[27]Imanaka, M., "Fatigue Strength of Adhesive/Rivet Combined Lap-joints," *Journal of Adhesion*, Vol. 49, Dec. 1995, pp. 197–209.

[28]Liu, J., and Sawa, T., "Stress Analysis and Strength Evaluation of Single-Lap Adhesive Joints Combining Rivets Subjected to External Bending Moments," *Reliability, Stress Analysis, and Failure Prevention Issues in Adhesive and Bolted Connections*, *ASME Proceedings*, Vol. 105, American Society of Mechanical Engineers, Fairfield, NJ, 1999.

[29]Dechwayukul, C., Rubin, C., and Hahn, G.,"Analysis of the Effects of Thin Sealant Layers on Aircraft Structural Joints," *AIAA Journal*, Vol. 41, No. 11, 2003, pp. 2216–2228.

[30]Li, G., and Shi, G., "Effect of the Riveting Process on the Residual Stress in Fuselage Lap-joints," *Canadian Aeronautics and Space Journal*, Vol. 50, No. 2, 2003, pp. 91–105.

[31]Markiewicz, E., Langrand, B., Deleotombe, E., Drazetic, P., and Patronelli, L.,"Analysis of the Riveting Forming Mechanisms," *International Journal of Materials and Production Technology*, Vol. 13, Nos. 3–6, 1998, pp. 123–145.

[32]"ABAQUS/Standard 6.4 User's Manual," Hibbitt, Karlsson, and Sorensen, Inc., Pawtucket, RI, Dec. 2003.

[33]Langrand, B., "Experimental Characterization of 2024-T351 and 7050 Aluminium Alloys," ONERA-Lille Rept. 97/54, Oct. 1997.

[34]Li, G., and Sullivan, P. L., "Finite Element and Experimental Studies on Single-Lap-joints in Tension," *Journal of Adhesion and Adhesives*, Vol. 21, Dec. 2001, pp. 211–220.